Alma Mater Studiorum Università di Bologna
Archivio istituzionale della ricerca

Experimental and numerical characterization of hydrogen jet fires

(Article begins on next page)

18 February 2025

Experimental and Numerical Characterization of Hydrogen Jet Fires

Mattia **CARBONI**[1]*, Gianmaria* **PIO**[2]*, Paolo* **MOCELLIN**[1]*, Francesco* **PILO**[3]*, Chiara* **VIANELLO**[1,4]*,*
Paola **RUSSO**[5]*, Giuseppe* **MASCHIO**[1]*, Ernesto* **SALZANO**[2,*]

[1] Dipartimento di Ingegneria Industriale, Università degli Studi di Padova. Via Marzolo 9, 35131, Padova, Italia

[2] Dipartimento di Ingegneria Civile, Chimica, Ambientale e dei Materiali, Università degli studi di Bologna, Via Terracini 28, 40131, Bologna, Italia

[3] Corpo Nazionale dei Vigili del Fuoco Comando Venezia. Via Motorizzazione 7, 37100, Venezia, Italia

[4] Dipartimento di Ingegneria Civile, Edile e Ambientale. Via Marzolo 9, 35131, Padova, Italia

[5] Dipartimento Ingegneria Chimica Materiali Ambiente. Università degli Studi di Roma La Sapienza. Via Eudossiana 18, 00199 Roma, Italia.

*Author to whom correspondence should be addressed: ernesto.salzano@unibo.it

Abstract

Compressed hydrogen gas is considered the most convenient and robust technological solution for long-term storage. However, several safety concerns are still under investigation. This work presents an experimental and numerical characterization of the jet flame produced after the accidental release from a high-pressure tank containing pure hydrogen at pressures ranging from 90 to 450 bar and release diameters ranging from 1 to 5 mm. Results are expressed in terms of temperature history and flame length. The complete set of measurements has been reported in the supplementary materials. Both integral and discrete models were employed. Besides, the computational fluid dynamic was integrated with finite reaction rate and accurate thermodynamic properties (from the *ab initio* approach) and showed excellent agreement with experimental data.

Keywords: Compressed Hydrogen; Jet fire; Experimental Campaign; Computational Fluid Dynamics; Ab initio; Flame Length.

Highlights:

- Experimental characterization of hydrogen jet fires up to high-pressure storage
- Comparison of experiments, empirical correlations, and computational fluid dynamics
- Integration of thermodynamic properties of compressed hydrogen calculated *ab initio*
- Estimation of the effect of boundary conditions on the flame length
- Evaluation of chemical and turbulence sub-models for hydrogen jet flames

Nomenclature

Symbols

D [mm]	Diameter		P [bar]	Pressure
C	Mole fraction of the unreacted fuel		$\dot{Q}$ [kW]	Power
CFD	Computational Fluid Dynamics		QM	Quantum mechanics
Fr	Froude Number		Re	Reynolds number
g [m s^{-2}]	Gravity acceleration		t [s]	Time
H [m]	Height		T [°C]	Temperature
L [m]	Length		u [m s^{-1}]	Velocity
M [kg]	Mass		W [m]	Width
$\dot{m}$ [kg s^{-1}]	Mass flow rate		X [m]	Distance from the releasing point

Subscripts and superscripts

ad	Adiabatic conditions		max	Maximum
AN	Actual nozzle exit parameters		p	Phenomenon
Eff	Effective (notional) nozzle		R	Rising phase
f	Flame		S	Surrounding air
Far	Far-field thermocouples		s	Source
IR	Infrared region		st	Stoichiometric condition
N	Nozzle		UV	Ultraviolet region
Near	Near-field thermocouples		w	Wind

Greek letters

α_T	Ratio of stoichiometric coefficients of reactants and products
α	Constant factor
Δh_c [kJ kg^{-1}]	Heat combustion
ρ [kg m^{-3}]	Density
μ [kg m^{-1} s^{-1}]	Dynamic viscosity

1. Introduction

The peculiar physical and chemical properties of hydrogen require tailor-made solutions addressing combustors, storage, and transportation systems. For storage, compressed hydrogen is currently the most convenient and robust solution, with an operating pressure up to 1000 bar [1]. However, uncertainties on safety issues arise when the operating pressure exceeds 350 bar, mostly due to the scarcity of experimental data related to the accidental scenario generated by the release of hydrogen and the subsequent ignition, i.e., jet fire. An overview of the state of the art of available data and models is provided in the following section. Current trends and future perspectives were reported and interpreted to individuate the most significant conditions to be investigated. Based on these findings, the accidental release of compressed hydrogen at pressures ranging from 90 bar to 450 bar through a nozzle whose internal diameters ranged from 1 to 5 mm was experimentally and numerically analysed in this work.

According to the current literature [2], the high pressure may cause significant deviations from the real behaviour and the one described by currently adopted thermo-physical correlations, thus suggesting the implementation of properties calculated through accurate and theoretically derived approaches, such as quantum chemistry [3]. To this aim, the *ab initio* approach should be mentioned since it derives from first principles and requires universal physical constants, only. This method attempts to solve the Schrodinger equation by identifying the most stable (i.e., lower energy) spatial configuration of the investigated molecules and expressing partial differential equations in algebraic equations through a linear combination of a set of basis functions. The latter step is essential for the effective implementation of this method in computational sources. In this perspective, the appropriate selection of the level of theory and basis sets to be used is essential to guarantee optimized results in terms of computational time and accuracy [4] [53]. A detailed description of the available techniques for *ab initio* calculations is out of the boundaries of this work. However, Readers can refer to the dedicated literature [5] [6] [7] to find detailed descriptions of the fundamental assumptions and common practices adopted in this field.

This work presents an integrated analysis combining experimental tests, empirical correlations, as well as detailed numerical models considering theoretically derived physical properties. To the best of our knowledge, this study reports the first attempt to implement the latter approach for the characterization of jet fires. The comparison of the accuracy of different numerical approaches can be intended as an essential step for the characterization of hydrogen storage systems using elevated pressure. The acquired knowledge can help the development of safe solutions and procedures, bringing new elements to support the decision-making process on hydrogen technologies.

2. Compressed hydrogen jet fire

An accidental release of compressed hydrogen through nozzles behaves as a choked flow jet if the expansion ratio is larger than 41.2 and as sonic in the range between 4.1 and 41.2 [8]. Due to its high reactivity, hydrogen jets are very likely to be ignited [9]. To characterize this scenario, several experiments have been conducted over the years [10–20]. Economic aspects have pushed for an increase in operative pressure, posing new challenges from a technological perspective [1] and significantly affecting the investigated ranges from a scientific point of view (Figure 1). Similarly, the realization of robust practices and procedures for safe design and operations have drastically changed the typical nozzle diameter (D_N) of interest for a possible release (Figure 1). Indeed, most of the recent measurements are focused on D < 5 mm.
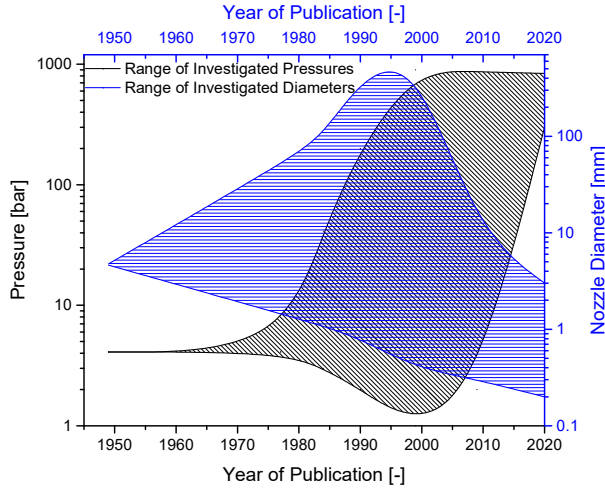
Figure 1. Qualitative representation of the trends for investigated pressure and nozzle diameter experimentally investigated for the characterization of jet fires along the years [10–20].

Once ignited, a crucial parameter is the flame size or flame length L_f, which is defined by the reaction (combustion) zone and, for most hydrocarbons, is coherent with the visible flame [21]. Quite often, in the common practice, L_f is calculated by several correlation originally derived from the classical theory proposed by Hawthorn et al. (1949) [10] [2]. However, this approach is only valid in the buoyancy-controlled flow regime and sets that L_f is proportional to D_N and some thermochemical characteristics of the substance: the ratio between the stoichiometric coefficients of reactants and products α_T, the adiabatic flame temperature T_{ad}, the fluid temperature at the nozzle T_N, the mole fraction of the unreacted fuel at the stoichiometric concentration in air C_{st}, and the mass ratio of the air and the flammable gas M_S/M_N. Subsequently, Shevyakov and Komov (1977) [11] have demonstrated that the correlation $\frac{L_f}{D_N}(F_r)$ is valid either for buoyancy or momentum controlled regimes, where F_r is the Froude number defined in Equation 1.

$$F_r = \frac{u_s}{\sqrt{g \cdot L_p}} \tag{1}$$

where u_s is the velocity of the source term, g is the gravitational acceleration, and L_p is the characteristic length of the phenomenon, namely the nozzle diameter in this case. Delichatsios (1993) [22] also studied the flame length relationships ranging from buoyancy to momentum-controlled and reported a maximum value of $L_f/D_N = 210$ for expanded hydrogen jets in the air. Kalghatgi et al. [12] performed more than 70 tests with subsonic and sonic hydrogen jet flames from a nozzle with diameters ranging between 1.08 mm and 10.1 mm. It was found that for subsonic and sonic flows L_f increases with the mass flow rate ($\dot{m}$) at fixed D_N, thus in contrast with the findings reported by Hawthorn et al. (1949), which does not report any correlation with $\dot{m}$. To this regard, Mogi et al. (2005) [13] studied subsonic, horizontal hydrogen jet flames from nozzles with a diameter ranging from 0.1 to 4.0 mm and pressure in the range of 0.1 to 400 bar. The work derived that the dimensionless flame length increases with the pressure P (expressed in bar), and they confirmed the dependence of L_f on $\dot{m}$. Later, Schefer et al. (2006) [14] conducted a series of vertical tests that permitted to find correlations between the L_f and the flame width (W_f), and between the length in the infrared (L_{IR}) and ultraviolet regions (L_{UV}). In addition, in 2007 the same research group published additional data on vertical jet flames for both subsonic and sonic flow at pressures up to 172 [15]. Based on mass and momentum conservation, these authors estimate the effective (notional) nozzle parameters (D_{eff}) considering the peculiar behaviour of hydrogen at high pressures, assuming no viscous forces, ambient pressure, and uniform velocity profile across the notional nozzle, sonic flow at the jet exit from the actual nozzle, and isentropic flow

relations [15]. In this relation, it is distinguished the actual nozzle exit parameters (AN) from the effective (notional) nozzle parameters (eff), and it considers the density (ρ). Later, in 2008, Imamura et al. [16] conducted a series of experiments to investigate the thermal hazards of hydrogen jet flames for exit pressures ranging from 5 to 30 bar. In 2009, Proust et al. [17] conducted an experimental campaign on horizontal hydrogen jet flame in a range of pressures from 10 to 900 bar and nozzle diameters from 1 to 10 mm. Temperature and mass flow rate were measured using K-Type thermocouples and a weighting device. Experimental data were used to calculate $\dot{m}$ and other flow parameters at the exit surface by the under-expanded jet theory [23]. The analysis concluded that experimental and theoretical results were in remarkable agreement. In the same years, other experimental tests on horizontal hydrogen jet fires were conducted by Studer et al. (2009) [18]. For the sake of conciseness, only the main characteristics of the above-mentioned experiments were reported in Table 1 and Figure 2. However, further information can be found in the current literature [24].

Table 1 Main characteristics of the experiments investigated from literature.

Source	Pressure (P) [bar]	Nozzle diameter (D_N)[mm]	Flame length (L_f)[m]	Proposed correlations
Hawthorn (1949) [10]	< 41	~4.7	[0.6 - 0.7]	$L_f/D = \dfrac{5.3}{C_{st}}\sqrt{\dfrac{T_{ad}}{\alpha_T T_N}\left[C_{st}(1+C_{st})\dfrac{M_S}{M_N}\right]}$
Shevyakov and Komov (1977) [11]	< 41	[1.4 - 51.7]	[0.3 - 1.7]	$\left(L_f/D\right)Fr$
Kalghatgi et al. (1984) [12]	< 41	[1.1 - 10.1]	[0.2 - 1.7]	$L_f(\dot{m})$
Mogi et al. (2005) [13]	[3 - 1100]*	[0.4 - 4.0]	[0.6 - 6.0]	$L_f/D = 524 \cdot P^{0.44}; L_f = 20.2 \cdot \dot{m}^{0.53}$
Schefer et al. (2006) [14]	[41 - 112]	[1.9 - 7.9]	[0.3 - 4.3]	$W_f = 0.2L_f; L_f = 0.9L_{IR}; L_f = 0.8L_{UV}$
Schefer et al (2007) [15]	[7 - 262]	5.1	[2.4 - 10.0]	$D_{eff} = D \cdot \sqrt{\dfrac{\rho_{AN}u_{AN}}{\rho_{eff}u_{eff}}}$
Imamura et al. (2008) [16]	[2 - 30]*	[1.0 - 4.0]	[0.3; 1.8]	
Proust et al. (2009) [17]	[12 - 869]	[1.0 -3.0]	[1.3 - 5.8]	Under expanded jet theory applied to calculate $\dot{m}$.
Studer et al. (2009)[18]	[2 - 83]	[4.0 - 10.0]	[1.7 - 6.9]	

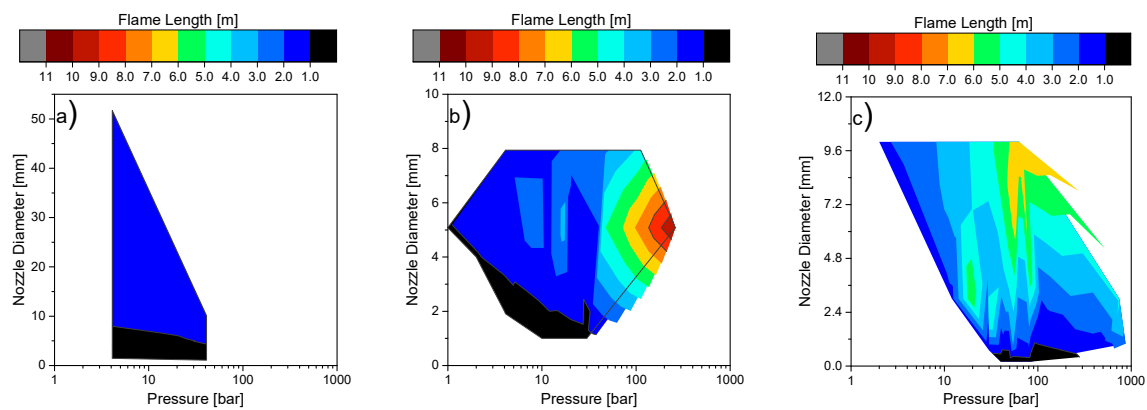*spouting pressures (static pressure measured close to nozzle exit)*

Figure 2. An overview of flame length (Lf) measured at different nozzle diameters and pressures as a function of the published year. More specifically, a) includes data published before 1985; b) data published from 1985 to 2008; and c) data published from 2009 on [10–20].

These studies represent part of the database commonly used to develop empirical correlations. In this sense, Molkov et al. [2] published a dimensionless correlation, which includes the dependence of flame

on both nozzle diameter and mass flow rate. Based on these results, the same authors [25] have found empirical correlations for the flame length L_f in the case of subsonic, sonic, and supersonic hydrogen jet flames (Equation 2).

$$L_f = \alpha \cdot (\dot{m} \cdot D_N)^{0.347} \qquad \dot{m}\ [kg\ s^{-1}]; D\ [m] \qquad\qquad (2)$$

where α is a constant factor equal to 76 for the best fit and 116 for representing the upper limit curve for the abovementioned experimental results. This equation has resulted as the most effective in reproducing a large set of experimental data and will be adopted in the following.

Hydrogen release and the diffusive combustion phenomena characterizing the jet flame can be studied by detailed numerical approaches [26] [27] [28]. Besides, due to the difficulties and risks associated with the experimentation with hydrogen, simulations have become a crucial tool for studying complex scenarios [29] [30] [31]. A certain number of numerical studies on hydrogen can be found in the literature in this framework. As an example, fundamental investigations on hydrogen atmospheric dispersion and combustion in different geometries have been approached numerically [32–34]. Several studies have also been performed on the modelling of high-pressure hydrogen jet flames, with the application of turbulence models including the k-epsilon, the Reynolds stress equation model, and the Large Eddy Simulation mathematical model for turbulence [35–37].

It generally emerges that although computational tools can potentially predict different aspects of hydrogen release scenarios with reasonable accuracy, they often demand a validation commitment, hence further experiments [38,39]. Besides, data for large-scale, pressurized release of hydrogen and correlated jet fires remain scarce because of safety concerns in large-scale experimental campaigns. Indeed, most of the current hydrogen validated experiments remain limited to small volumes or scaled trials [40].

3. Methodology

3.1. Experimental procedure

The experimental campaign reported in this work was performed in collaboration with the Italian National Fire and Rescue Service, and it follows a former set of experiments carried out with pressurized hydrogen [1]. The experiments consisted of horizontal releases of hydrogen, 1 m above the ground, ignited by a methane-based burner. The adopted experimental set-up can be intended as composed of subsections devoted to hydrogen storage, hydrogen discharge, and data collection. The storage section consisted of 16 bottles with a volume of 50 l each and initial pressure (P) of 450 bar, filled with hydrogen at 5N purity. A 15 m pipe with a constant internal diameter (D) of 7 mm connected to nozzles of different sizes, namely 1, 3 and 5 mm, was used as per the discharge subsection (Figure 3). The last subsection gathered data for the wind speed and direction as well as temperature distribution and IR images.
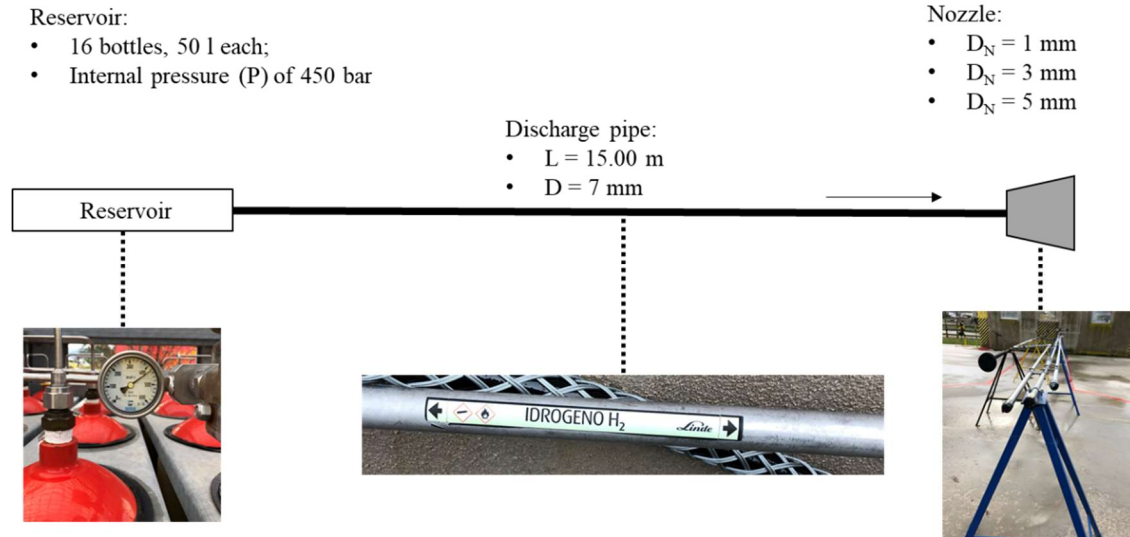
Figure 3. Schematic representation of the system used to release compressed hydrogen.

The wind speed and direction were logged at the height of 3 m by an onsite mobile weather station. The wind direction was mostly coincident with the direction of the jet (i.e., north) during the entire campaign. An arrangement of 16 type-K thermocouples with an estimated accuracy of $\pm$ 2.5 °C [21] was realized to record the temperature distribution with a data acquisition rate of 30 samples per second. Figure 4 reports a schematic representation of the location of thermocouples, distinguished into two groups according to the distance from the release point.
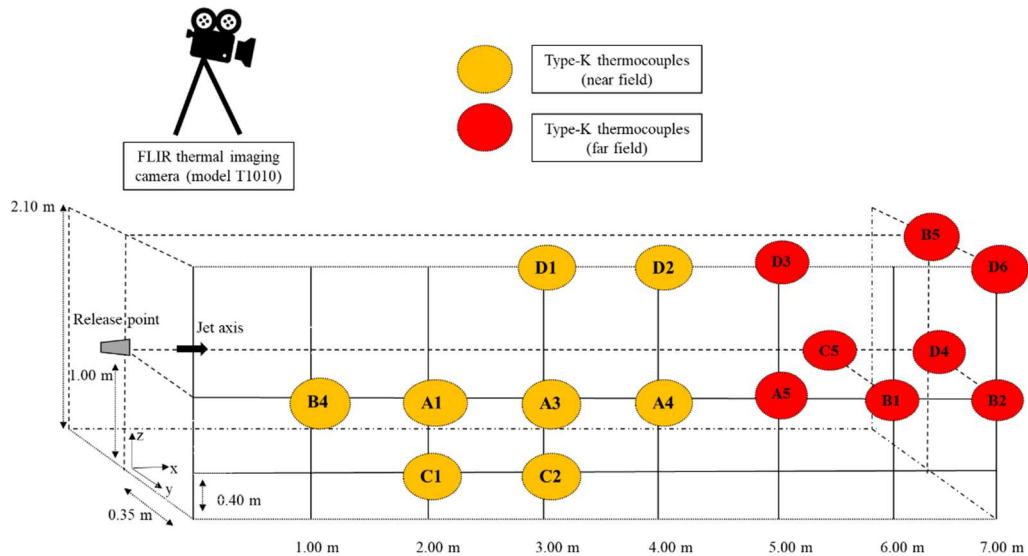

Figure 4. Schematic representation of the arrangement of thermocouples. Thermocouples named near-field are indicated in orange, whereas in red far-field thermocouples.

Besides, the flame structure was characterized by visible and infrared (IR) digital images recorded during the experiments. They were collected using a FLIR thermal imaging camera (model T1010) with an accuracy of $\pm$ 2 °C in all the investigated temperature ranges. The storage video frame rate of the images was 30 Hz. IR images are helpful to determine flame regions of high temperature since the emission in the infrared results primarily from the vibration of H_2O molecules produced in high-temperature combustion processes [18]. More in detail, each thermal image was analyzed, considering a frame representative of the steady-state phase. The accuracy of both the thermocouples and the thermal imaging camera (i.e., $\pm$ 2.5 °C and $\pm$ 2.0 °C, respectively) do not significantly affect the

accuracy in estimating the jet flame L_f. At most, an incidence of 0.003% is expected when investigating the flame region (i.e., for temperature higher than 800 °C). Overall, 17 tests were performed at different nozzle diameters (D_N) and the initial storage pressure (P), as reported in Table 2.

Table 2. Experimental tests reported in the present work and main conditions. Measured environmental temperature $T_a^o = 16 \pm 2\,°C$.

Test	Nozzle diameter (D_N) [mm]	Initial pressure (P) [bar]	Wind velocity (u_w) [$m\,s^{-1}$]
#1		365	1.0
#2	1	360	0.5
#3		350	0.5
#4		450	2.0
#5		420	2.0
#6		380	2.0
#7	3	340	1.0
#8		300	2.0
#9		270	0.0
#10		240	1.0
#11		220	0.5
#12		340	0.0
#13		270	2.0
#14	5	240	0.5
#15		125	2.0
#16		120	2.0
#17		90	1.5

For the sake of this work, the flame length L_f was assumed as the maximum horizontal distance from the nozzle at which a temperature of 600 K is registered, in accordance with the current literature [41].

Since the adopted approach investigates transient phenomena, a typical trend characterized by an initial pseudo-steady state followed by decay is expected. Hence, attention was posed to identifying the rising and the steady-state phases of the investigated scenario. The steady-state has been considered as the phase where the temperature variation rate (dT/dt) was lower or equal to 5% of the maximum value of the temperature variation $(dT/dt)_{max}$ [42].

To evaluate the fluid dynamic data at the outlet, the isothermal turbulent choked gas steady jet theory was applied [43], as suggested by Vianello et al. [1]. A turbulent gas jet propagates from the stagnant condition inside the containment to the zone where a different pressure generates the fuel release. It is worth noting that the gas velocity is chocked. Hence, if the upstream pressure increases, the mass flow rate increases due to the density rise, not due to the velocity rise [55]. Then, the initial momentum is lost, and the flow becomes predominantly governed by other agents, such as buoyancy and wind. Hence, after an initial and horizontal phase, the flame develops vertically. The retrieved $\dot{m}$ was used to apply the empirical correlation expressed by Eq. 2 ($\alpha = 76$) and consequently to obtain the empirical length flame. Moreover, the value of $\dot{m}$ was used to estimate the power $\dot{Q}$ (Equation 3) produced by the hydrogen jet fire, considering the hydrogen heat combustion Δh_c equal to 119.96 $kJ\,kg^{-1}$ [44]:

$$\dot{Q} = \dot{m} \cdot \Delta h_c \tag{3}$$

Finally, the maximum distance at which the threshold temperature for a third-degree burn (i.e., 300 °C) is reached ($X_{300°C}$) was calculated for the sake of completeness [2].

3.2. Modelling approach

Numerical evaluations were performed using either integral models [45] or computational fluid dynamics (CFD) [46]. The former includes the SHELL jet fire calculation method [47] [48] to estimate the shape and power of the flame. The adopted equation is typically included in commercial codes for the consequence assessment, whereas the latter uses the licensed software ANSYS Fluent. In both cases, several tests were performed to consider each atmospheric condition registered during the experimental campaign. For the CFD case, the numerical domain was characterized by length (L) and height (H) of 12 m and 5.5 m, respectively. The extension of the domain was chosen by analyzing the thermal images and defining the full development of the hydrogen jet fire. Regarding the employed mesh, it was decided to divide the domain to facilitate a more accurate concentration of the mesh elements in the areas where a higher momentum was expected. Based on grid sensitivity analysis, a total of 511949 nodes and 510787 elements were selected as optimized parameters. Hence, this setup was used for the following analyses (Figure 5).
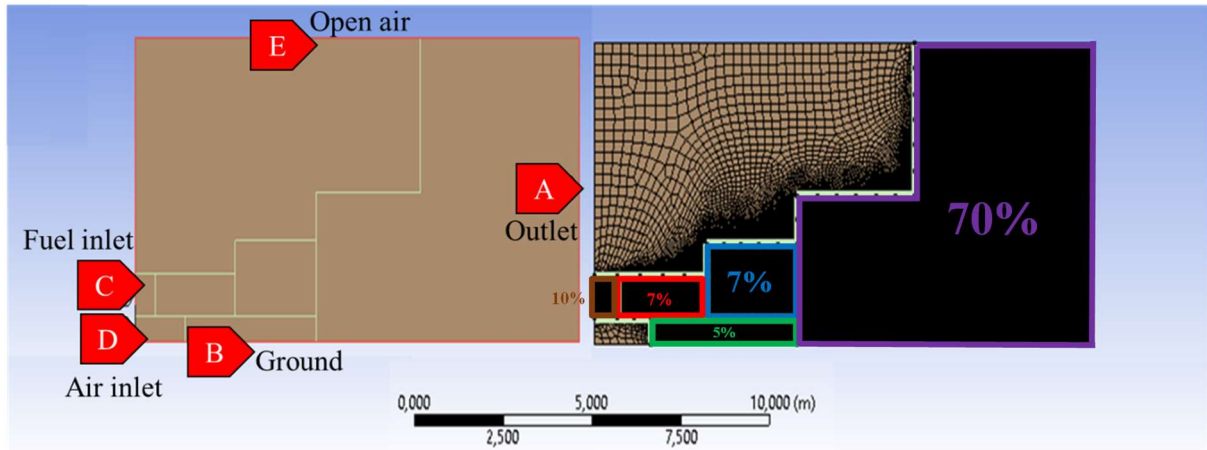

Figure 5. Representation of the numerical domain (left) and the mesh grid (right) adopted for the computational fluid dynamic analyses. The percentages of elements allocated for the main sections are reported. Please consider that they account for ~99% of the total number of elements.

The outflow conditions were applied to the upper (E, open-air) and right (A, outlet) sides of the domain while to the lower part (B, ground) was applied the wall. An inlet velocity was imposed to the left side (D, air inlet), except for the C portion (fuel inlet), where the mass flow inlet was calculated based on the investigated pressure. Indeed, in C, an initial gauge pressure (i.e., the static pressure [49]) was defined following the experimental test to be mimicked. Additional information on the adopted sub-models can be retrieved in the supplementary materials. Two different strategies were tested to evaluate the thermodynamic properties of the involved species: the use of empirical-based coefficients and the implementation of theoretically derived coefficients. The former implements the existing database present in the adopted CFD software, whereas the latter (referred to as CFD model + QM from now on) uses a combination of coefficients deriving from *ab initio* calculations. More specifically, data reported in the literature for nitrogen, oxygen, and low-temperature interval for hydrogen [50] were integrated with water and high-temperature parameters for hydrogen [51], where the CBS-QB3 level of theory and G3//B3LYP method were adopted, respectively. An elevated accuracy is attributed to both approaches [52]. The abovementioned coefficients refer to NASA polynomials expressed in a compact form in Equations 4-6 for the evaluation of heat capacity (c_p), enthalpy (H), and entropy (S) as a function of gaseous temperature (T).

$$c_p = R \cdot \sum_i^5 (a_i \cdot T^{i-1}) \tag{4}$$

$$H = (R \cdot T) \cdot \left[\frac{a_6}{T} + \sum_i^5 \left(\frac{a_i \cdot T^{i-1}}{i} \right) \right] \tag{5}$$

$$S = R \cdot \left[a_1 \cdot \ln(T) + a_7 + \sum_i^4 \left(\frac{a_{i+1} \cdot T^i}{i} \right) \right] \tag{6}$$

where R stands for the ideal gas constant and a_i for the i-th coefficient. The thermodynamic databases provide two values per coefficient a_i to distinguish low-temperature (e.g. for T ≤ 1000 K) and high-temperature (e.g. for T > 1000 K) ranges, following the approach commonly used [53].

4. Results and discussion

4.1. Experimental results

For a matter of brevity, only a reduced number of data was discussed and reported in this section. The complete set of measurements has been reported in the supplementary materials. To provide insight on the flame structure and involved phenomena, a focus on Test #5, identified as a base case for this study, was provided at first.

Figure 6 shows the IR image related to Test #5 (initial pressure of 420 bar and nozzle diameter 3 mm) at the steady-state condition. The IR image of all other tests reported in Table 1 can be found in the supplementary materials (Figures S17-S32). Four different temperature zones were distinguished (intense red, light red, orange, and yellow) corresponding to the temperature ranges T > 1400 °C, 800 °C < T < 1400 °C, 600 °C < T < 800 °C, and T < 400 °C. Cool combustion products can also be seen outside the jet shape (white colour).
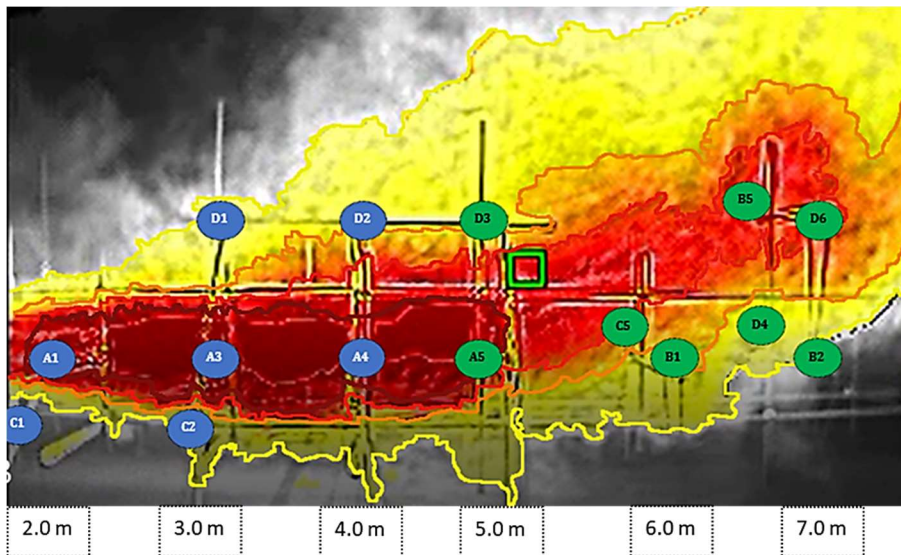

Figure 6. IR image measured for Test #5 at steady state. Four zones are distinguished: T > 1400 °C (dark red), 800 °C < T < 1400 °C (red), 600 °C < T < 800 °C (orange), and T < 400 °C (yellow).

As expected, the momentum forces prevail on the buoyancy ones in the first region, followed by a buoyancy-regulated flame once the density of the plumes is significantly decreased by the occurrence of combustion phenomena. The geometry of the second region can be fairly described by assuming a tilt angle of ~ π/6 to the releasing direction (i.e., horizontal axis). In this perspective, the evaluation of the length of the first region is essential to properly describe the frustum of the flame. It should be noted that this parameter increases with a larger nozzle for any given pressure. This trend can be attributed to the enhanced volume to external surface ratio of the core area due to an increase in the nozzle diameter. Indeed, the assumed modification in the geometry of the flame positively influences the power generation and has a detrimental effect on heat transfer ruling, thus modifying the spatial evolution of the density of the gaseous mixture within the core. The length of the momentum-dominated region is weakly affected by the initial pressure if the tests based on a nozzle of 5 mm are neglected. Indeed, it can be fairly considered equal to 5 m for Test #5 and any tests conducted in this work with a nozzle

diameter of 3 mm and 3 m for tests using a nozzle diameter of 1 mm. Conversely, the effect of pressure observed for tests using a nozzle diameter of 5 mm is relevant once the initial value is lower than 200 bar (i.e., Tests #15 - 17). An explanation for this behaviour may stand behind possible mass transfer limitations and reduced turbulence, limiting the availability of reactants and mixing efficiency, thus slowing the combustion rates.

Figure 7 shows the experimental temperature measured during Test #5 at different locations by the thermocouples.
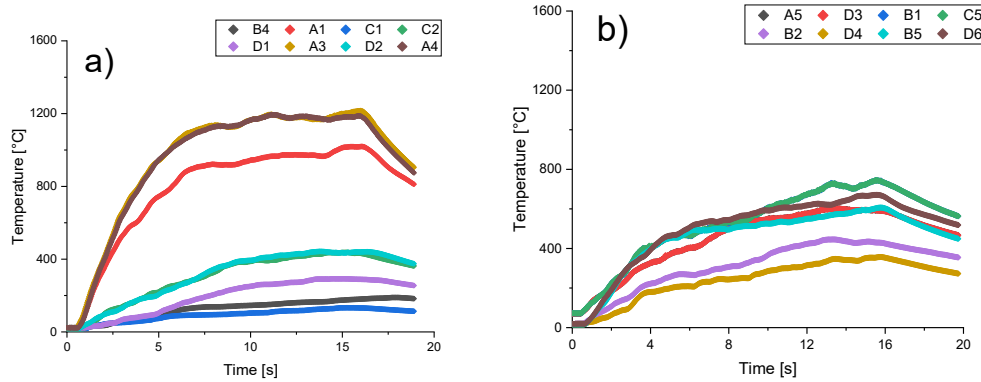

Figure 7. *Measured temperature history at different locations for Test #5 (initial pressure 420 bar and nozzle diameter 3 mm). a): near field; b): far-field.*

Following the typical jet fire description, which is still valid for hydrogen, the measured temperature is characterized by an initial temperature rise, followed by a profile stabilization at the maximum temperature. Hence decay is observed after the flow was stopped due to the residual pressure. Similar trends can be observed for any thermocouple and any test, as reported in Figures S1-S16 of the supplementary materials.

Measured temperatures collected in this work during different tests as a function of distance X from the releasing point were compared with data from the literature in Figure 8. To make the obtained results compared with data from the literature [54] [16] [55], the results were normalized to the corresponding flame length L_f. For the sake of clarity, among the newly collected data only the ones corresponding at X/L_f equal to 1 and $X_{300 °C}/L_f$ were reported in Figure 8.
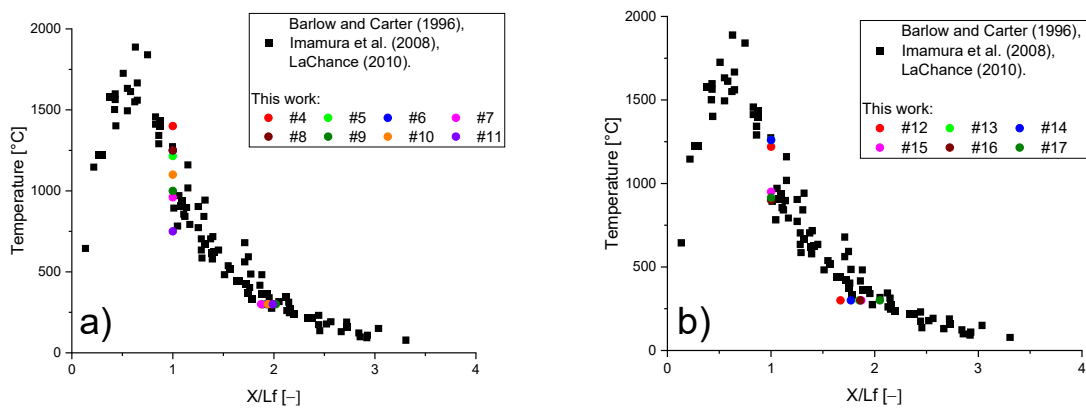

Figure 8. *Maximum temperature as a function of distance from the nozzle (X) normalized by the flame length L_f, as obtained for 3 mm nozzle diameter (a) and 5 mm nozzle diameter (b). Black squares represent experimental data from the current literature and, more specifically, by Barlow & Carter (1996) [54], Imamura et al., (2008) [16], LaChance, (2010) [55].*

The experimental data collected in this work comply with the trends observed in the literature: either the pressure or the nozzle size may significantly affect the extension of flame. The IR images reported

in supplementary materials show a flame core area in which peaks in temperature are expected in the proximity of $0.5 \cdot L_f$. In this zone, the maximum temperature range measurable in our campaign (i.e., higher than 1400°C) was recorded; thus, peaks of ~ 2000 °C cannot be excluded. This temperature and the relative positions agree with several experimental data reported in the cited literature. For example, for a 1 mm nozzle diameter, the IR images at different initial pressure (Figures S17-S19) show that the dark red zone is not present, and the red zone reaches 2 m in length for any pressure investigated in this work. Conversely, the sizes of the other zones significantly change with the initial pressure and constant nozzle diameter. On the other hand, the dark red zone can be detected in the case of larger diameters.

The effect of the diameter on the temperature field was observed by comparing the temperature history for Tests #3, #7, and #12, which have similar initial pressure (i.e., ~350 bar) and different nozzle diameter (e.g., 1, 3, and 5 mm) (Figure 9).
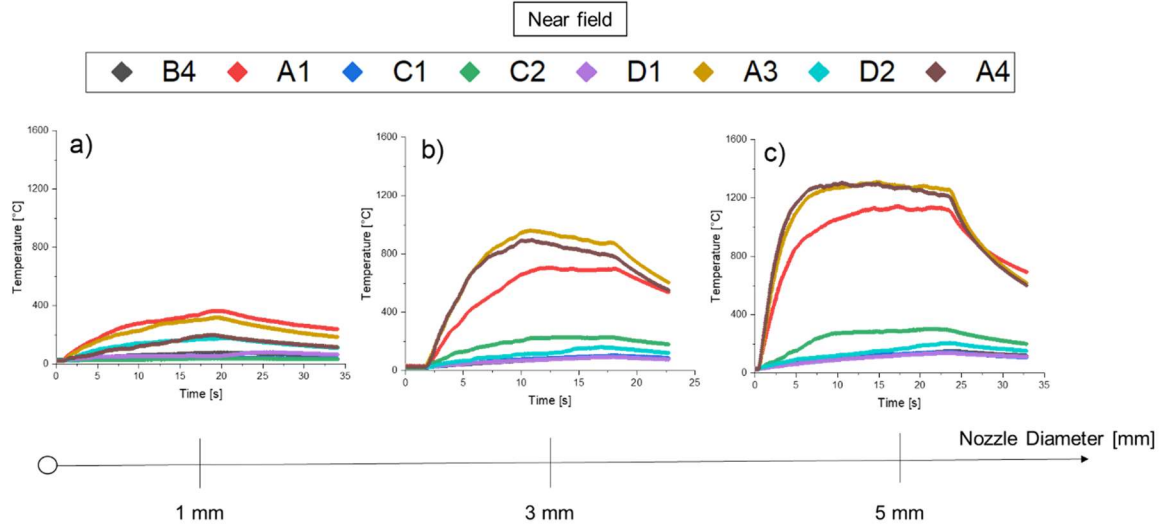

Figure 9. Measured temperature history at different locations in the near field group of thermocouples for Test #3 (a), Test #7 (b), and Test #12 (c).

An overall general increase in the temperatures is registered between 1 mm and the other diameters, reaching a variation up to 850 °C. On the other hand, no particular differences were observed between Test #7 (3 mm) and Test #12 (5 mm) for the spatial distribution of the temperature. In the case of 1 mm, the maximum temperature was registered by thermocouple A1 which in the other tests was always recorded lower temperature in the other cases. These discrepancies can be mainly attributed to the different initial conditions, resulting in lower momentum at the releasing point. Hence, the nozzle diameter significantly affects the length of the buoyancy area and the flame shape.

The effects of the initial pressure for a given nozzle diameter on measured temperature were analysed by comparing results obtained in conditions described as Tests #4, #8, and 11#, hence with a diameter of 3 mm (Figure 10). Similarly, the obtained estimations under the corresponding initial conditions are reported in Figure S33, where satisfactorily prediction quality can be observed as well as trends in line with the ones discussed in previous sections.
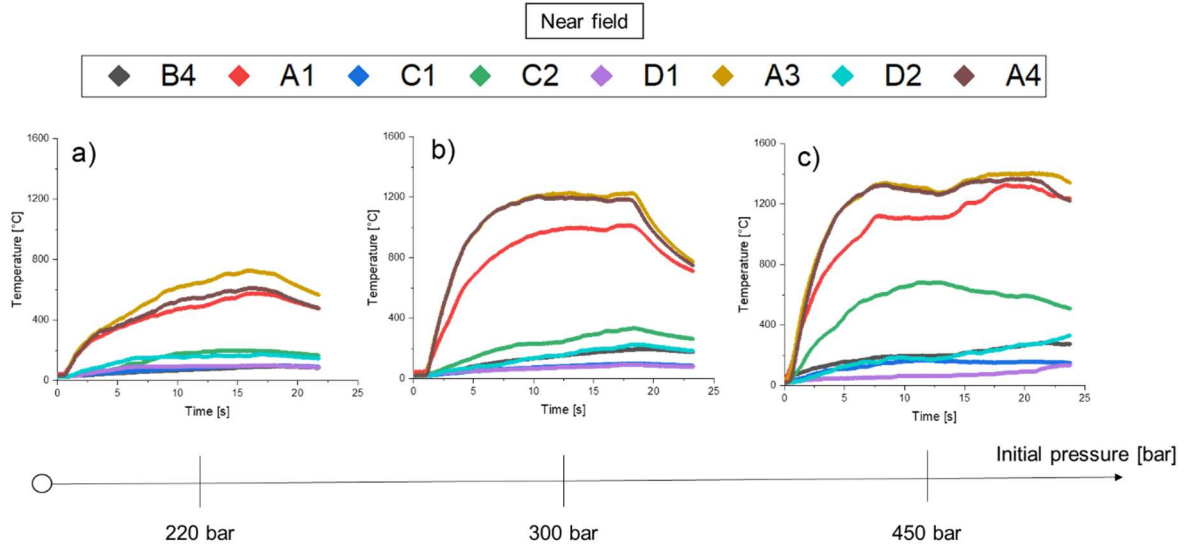
Figure 10. Measured temperature history at different locations in the near field group of thermocouples for Test #11(a), Test #8 (b), and Test #4 (c).

The characterization of flame structure can be performed by integrating the presented data with the maximum temperatures registered in time and space. For the sake of completeness, two regions were distinguished at this stage: near-field and far-field. Table 3 reports the experimental data collected in this work for the maximum temperatures recorded in the near and far-field by any thermocouples located in the combustion zone and the duration of the rising phase (t_R) for all the conducted tests. Besides the maximum distance at which the temperature reaches 300 °C ($X_{300 °C}$) is added.

Table 3. Maximum temperature measured in the near-field (T_{near}) and far-field (T_{far}), flame length (L_f), and duration of the rising phase (t_R). Also, the maximum distance at which the temperature reaches 300 °C ($X_{300°C}$) is reported. *Steady-state not reached. **Temperature reached only in the proximity of the flame.

Test	T_{near} [°C]	T_{far} [°C]	L_f [m]	t_R [s]	$X_{300°C}$ [m]
#1	250	190	2.4	5.8	**
#2	285	185	2.8	9.0	**
#3	370	290	2.5	*	3.0
#4	1400	900	6.2	4.5	8.5
#5	1215	780	5.8	6.1	8.5
#6	1250	720	5.2	6.2	8.3
#7	960	750	5.0	7.5	7.5
#8	1230	550	4.8	6.5	7.1
#9	980	680	4.7	8.9	7.1
#10	1100	400	4.8	13.9	6.0
#11	750	470	4.6	*	6.0
#12	1220	1050	5.8	5.0	10.0
#13	1260	650	6.7	3.5	10.0
#14	1260	700	5.3	3.5	7.1
#15	950	500	3.9	8.2	5.6
#16	900	550	3.7	0.8	5.4
#17	915	290	3.6	7.4	5.1

It is worth mentioning that, regardless of the investigated initial conditions, the maximum temperatures were recorded by thermocouples A3 and A4 in the near-field and by C5 in the far-field, showing the time evolution of the frustum of the flame.

For the 1 mm nozzle diameter (Tests #1÷ #3), the flame core was characterized by temperatures within 250 °C and 370 °C, which is the maximum temperature recorded in the near field, at 2.0 m from the nozzle. Hence, it can be concluded that these conditions cannot generate second cascading events involving storage tanks since the radiation flux resulting from the maximum recorded temperature, calculated following the Boltzmann equation, is significantly lower than the typical threshold values [56]. Conversely, second cascading events can be triggered by a release from a nozzle of 3 mm and 5 mm also in the region referred to as far-field. For the 3 mm nozzle diameter (Tests #4 ÷ #11), a maximum temperature of 1400 °C was observed, with temperatures ranging between 750 °C and 1400 °C within the flame core. Eventually, for the 5 mm nozzle diameter (Tests #12 ÷ #17), a maximum temperature of 1260 °C and a range between 900 °C - 1260 °C were reported. Besides, at far field, Test 12 is the only case where temperatures larger than 1000 °C were recorded although longer flames were observed under other experimental conditions. The reported data are in line with the trends discussed for the length of the momentum-dominated region, where the combination of parameters most affected by gaseous pressure (e.g., available reactants and mixing efficiency) and nozzle diameter (e.g., the surface to volume ratio) ruled the interactions between heat transferred and generated power.

4.2. Numerical results

A plot of the results obtained utilizing the CFD approach mimicking the conditions indicated as Test #5 is reported in Figure 11. Similarly, numerical results obtained at different pressures are reported in Figure S33.
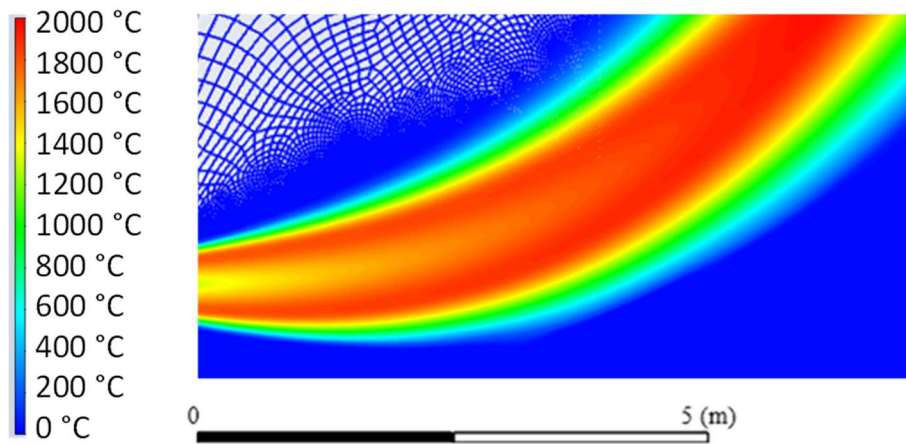

Figure 11. Estimated temperature distribution within the flame zone in conditions referred to as Test #5, as calculated by ANSYS Fluent.

Regardless of the investigated nozzle diameter, jets are characterized by source Froude number ($Fr_s = u_s/[(gD_s)^{0.5} \cdot (\rho_s/\rho_{air})]$) and Reynolds number ($Re = u_s \cdot D_s \cdot \rho_{air}/\mu_{air}$) higher than 50 and 1×10^5, respectively. The combination of these values implies the existence of a pure momentum turbulent condition having inertia controlled transition region under the classification proposed by Delichatsios (1993) [57]. Besides, a lift-off distance can also be assessed based on the temperature distribution. For these reasons, the temperature profiles resulting from the numerical investigation performed in this work for the Test #5 (420 bar; 3 mm) is reported in Figure 12 as a function of the height from ground H and the downwind distance.
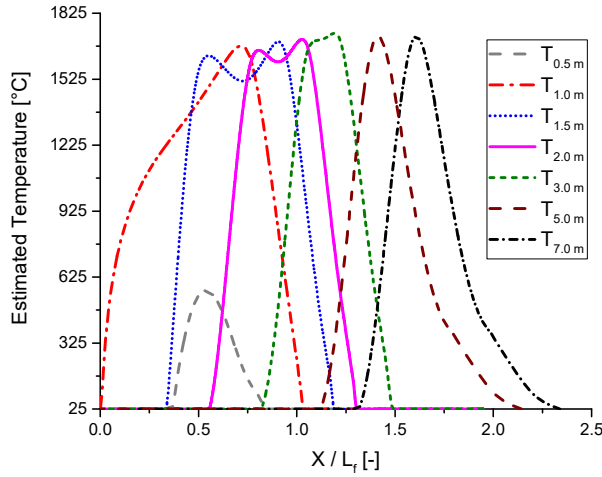
Figure 12. Estimated temperature as a function of distance from the nozzle (X) normalized by the flame length L_f (equal to 5.3 m), as obtained for 3 mm nozzle diameter. Please consider that subscripts reported in the legend refer to the height from the ground.

The maximum temperature achieved under the releasing point height is significantly limited, being lower than 600 °C, because of the physical properties of unburned and burned gases investigated in this work. If estimations at 1.0 m (i.e., the releasing height) and 1.5 m are considered, the maximum temperature is reached at $X/L_f \sim 0.5$, in compliance with indications provided in the section dedicated to experimental data. Besides, two peaks characterized by comparable temperatures can be observed at any curves reporting data at 1 m < H < 5 m, indicating that the fuel-rich pocket is crossed by the horizontal lines in this region. It is worth noting that second peaks reach higher temperatures in any curves because of the buoyancy effect and different thermal properties between substrates and air surrounding the flame. The distance between these peaks indicates that the abovementioned pocket has a maximum thickness slightly smaller than the flame length. Hence, a significant amount of hydrogen can be expected up to H = 5 m.

The reported conclusion is corroborated by the maximum hydrogen content to the distance from the releasing point ($H_{2,max}$), as estimated at different levels from the ground (H) (Table 4).

Table 4. Maximum hydrogen content to the distance from the releasing point ($H_{2,max}$) at different levels from the ground (H), as estimated by ANSYS Fluent for Test #5.

H [m]	0.50	1.00	1.50	2.00	3.00	5.00	7.00
$H_{2,max}$ [%mol]	0.11	97.12	20.48	14.87	8.05	0.89	0.10

4.3. Comparison of adopted approaches

The mass flow rate, the heat power produced by the hydrogen jet fire [44], and the flame length resulting from the empirical model (Eq. 2) considering the best fit ($\alpha = 76$) and the upper limit ($\alpha = 116$) can be retrieved in the supplementary materials (Table S2). In the same table, the total energy produced by the jet fire considering the total duration of the combustion phase is also reported.

For the sake of comparison, two different datasets were included for the ANSYS Fluent route: the thermodynamic coefficients included within the libraries (CFD model) and the thermodynamic coefficients resulting from quantum mechanical calculations (CFD model & QM). The 3 mm nozzle diameter was taken as a reference due to the larger availability of experimental results. It is worth noting that similar trends can be observed between experimental and numerical data once the maximum values at any distance X to height H for the latter case are considered. In this perspective, 300 °C and ambient temperatures can be observed at $x/L_f \sim 2.8$ and $x/L_f > 3$, respectively. On the contrary, if only the estimations resulting at $H = 1$ m are considered, both threshold temperatures are reached at $x/L_f < 1.5$,

with obvious implications for the safety analysis. The comparison of the flame length deriving from different approaches considered in this work is provided in Figure 13.
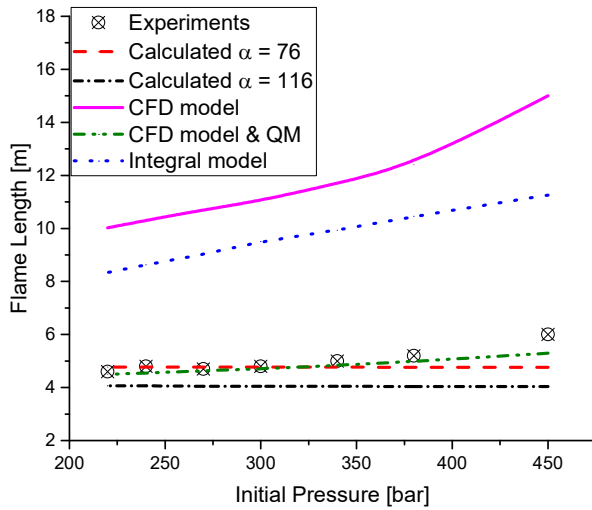

Figure 13. Comparison of the length flame (L_f) between measured values within the experimental campaign performed in this work and estimated values resulting by different methods, for the case of 3 mm nozzle diameter at a different initial pressure. Please consider that the calculated term refers to Equation 2, the CFD model refers to the case with standard thermodynamic coefficients, whereas the CFD model & QM refers to the case with ab initio derived properties; the Integral model refers to models reported in the literature [45].

The comparison between experimental and numerical results for the temperature distribution and flame length indicates that the adopted sub-models allow for fair estimations of large-scale scenarios, as well. Indeed, the numerical approach accurately describes the flame pattern, as demonstrated by similar flame patterns. More specifically, either initial jet expansion toward a height lower than the releasing point or lift-off distance is well captured by CFD. On the other hand, the tendency to over-predict the temperature should be noted. This discrepancy can be partially attributed to the lack of further distinctions in measured temperature above 1400 °C, or it may indicate an excess in generated heat, possibly due to the considered rates for the overall (apparent) reactions. Indeed, for the numerical case, the maximum temperatures approach the adiabatic flame temperatures due to the assumptions of the employed model for the evaluation of heat transfer phenomena. An almost linear trend between initial pressure and flame length can be observed for the estimation deriving from integral models. In this case, the length of flame is assumed as the maximum distance from the nozzle where the maximum heat radiation and temperature are reached, following the approach used for the definition of the experimental L_f. In contrast with the other approaches included in this work, the CFD model with default thermochemistry shows more than a linear trend with pressure. Furthermore, estimations deriving from integral models and CFD with default thermochemistry are significantly conservative on the safe side under any conditions considered. On the other hand, predictions determined by the CFD model with QM and the empirical approach are more accurate, demonstrating the effect of thermodynamic properties on one side and the validity of empirical correlations on the other side. Regardless of the implemented database for thermodynamic data, the positions indicated by the flame length correspond to the farthest with a non-negligible concentration of hydrogen in the direction perpendicular to the nozzle, thus representing an alternative criterion for evaluating the flame length in the case of CFD investigations.

5. Conclusions

This work presents an experimental and numerical investigation of the behaviour of hydrogen release from a high-pressure reservoir in the presence of an ignition source. The analysed scenario (i.e., jet fire) was characterized in terms of temperature evolution with time and space (distance from the releasing

point) and the terms of flame length. The effects of initial pressure and nozzle diameter on the measured properties were discussed given physical-chemical phenomena possibly characterizing the investigated scenario. The measured flame length was lower than 7.0 m for all the investigated pressures (90 – 450 bar) and release diameter (1 – 5 mm). An empirical correlation from the literature (Eq. 2) developed by a data fitting approach can fairly reproduce the newly collected data. However, standard numerical models tend to over-predict the flame length. Conversely, numerical results have demonstrated that CFD codes can accurately reproduce jet fire scenarios only if thermodynamic properties deriving from accurate *ab initio* calculations are implemented. Eventually, the CFD approach allowed for the estimation of flame structure within the area surrounding the releasing point.

Acknowledgements

Reference

[1]   Vianello C, Carboni M, Mazzaro M, Mocellin P, Pilo F, Pio G, et al. Hydrogen refueling stations: Prevention and scenario management. large scale experimental investigation of hydrogen jet-fires. Chem Eng Trans 2020;82:247–52. https://doi.org/10.3303/CET2082042.

[2]   Molkov V. Fundamentals of Hydrogen Safety Engineering I. vol. 4. 2012.

[3]   Carboni M, Pio G, Vianello C, Maschio G, Salzano E. Large eddy simulation for the rapid phase transition of LNG. Saf Sci 2021;133:105001. https://doi.org/10.1016/j.ssci.2020.105001.

[4]   Pickard FC, Pokon EK, Liptak MD, Shields GC. Comparison of CBS-QB3, CBS-APNO, G2, and G3 thermochemical predictions with experiment for formation of ionic clusters of hydronium and hydroxide ions complexed with water. J Chem Phys 2005;122:1–7. https://doi.org/10.1063/1.1811611.

[5]   McQuarrie DA, Simon JD. Physical Chemistry: A Molecular Approach. 1997. https://doi.org/10.1021/ja01419a806.

[6]   Becke AD. Perspective: Fifty years of density-functional theory in chemical physics. J Chem Phys 2014;140. https://doi.org/https://doi.org/10.1063/1.4869598.

[7]   Mardirossian N, Head-Gordon M. Thirty years of density functional theory in computational chemistry: an overview and extensive assessment of 200 density functionals. Mol Phys 2017:2315–72. https://doi.org/https://doi.org/10.1080/00268976.2017.1333644.

[8]   Ishii R, Fujimoto H, Hatta N, Umeda Y. Experimental and numerical analysis of circular pulse jets. J Fluid Mech 1999;392:129–53. https://doi.org/https://doi.org/10.1017/S0022112099005303.

[9]   Astbury GR, Hawksworth SJ. Spontaneous ignition of hydrogen leaks: A review of postulated mechanisms. Int J Hydrogen Energy 2007;32:2178–85. https://doi.org/10.1016/j.ijhydene.2007.04.005.

[10]   Hawthorne WR, Weddell DS, Hottel HC. Mixing and combustion in turbulent gas jets. Symp Combust Flame Explos Phenom 1948;3:266–88. https://doi.org/10.1016/S1062-2896(49)80035-3.

[11]   Shevyakov GG, Komov VF. Effect of noncombustible admixtures on length of an axisymmetric on-port turbulent diffusion flame. Combust Explos Shock Waves 1977;13:563–6. https://doi.org/10.1007/BF00742209.

[12]   Kalghatgi GT. Lift-off heights and visible lengths of vertical turbulent jet diffusion flames in still air. Combust Sci Technol 1984;41:17–29. https://doi.org/10.1080/00102208408923819.

[13]   Mogi, T.; Nishida, H.; Horiguchi S. Flame Characteristics of high-pressure hydrogen gas jet. First Int Conf Hydrog Saf 2005.

[14]   Schefer RW, Houf WG, Bourne B, Colton J. Spatial and radiative properties of an open-flame hydrogen plume. Int J Hydrogen Energy 2006;31:1332–40. https://doi.org/10.1016/j.ijhydene.2005.11.020.

[15]   Schefer RW, Houf WG, Williams TC, Bourne B, Colton J. Characterization of high-pressure, underexpanded hydrogen-jet flames. Int J Hydrogen Energy 2007;32:2081–93.

[16]   Imamura T, Hamada S, Mogi T, Wada Y, Horiguchi S, Miyake A, et al. Experimental investigation on the thermal properties of hydrogen jet flame and hot currents in the downstream region. Int J Hydrogen Energy 2008;33:3426–35. https://doi.org/10.1016/j.ijhydene.2008.03.063.

[17]   Proust C, Jamois D, Studer E. High pressure hydrogen fires. Int J Hydrogen Energy 2011;36:2367–73.

[18]   Studer E, Jamois D, Jallais S, Leroy G, Hebrard J, Blanchetière V. Properties of large-scale methane/hydrogen jet fires. Int J Hydrogen Energy 2009;34:9611–9. https://doi.org/10.1016/j.ijhydene.2009.09.024.

[19]   Sun CJ, Sung CJ, He L, Law CK. Dynamics of weakly stretched flames: Quantitative description and extraction of global flame parameters. Combust Flame 1999;118:108–28. https://doi.org/10.1016/S0010-2180(98)00137-0.

[20]   Kobayashi H, Muto D, Daimon Y, Umemura Y, Takesaki Y, Maru Y, et al. Experimental study on cryo-compressed hydrogen ignition and flame. Int J Hydrogen Energy 2020;45:5098–109. https://doi.org/10.1016/j.ijhydene.2019.12.091.

[21]   Palacios A, Rengel B. Flame shapes and thermal flux of vertical hydrocarbon flames. Fuel 2020;276. https://doi.org/10.1016/j.fuel.2020.118046.

[22]   Delichatsios M. Transition from momentum to buoyancy-controlled turbulent jet diffusion flames and flame height relationships. Combust Flame 1993.

[23] Molkov V, Makarov V, Bragin M V. Physics and modelling of underexpanded jets and hydrogen dispersion in atmosphere. Phys Extrem States Matter 2009:146–9.

[24] Molkov V, Saffers JB. The correlation for non-premixed hydrogen jet flame length in still air. Fire Saf Sci 2011:933–43. https://doi.org/10.3801/IAFSS.FSS.10-933.

[25] Molkov V, Saffers J. Hydrogen jet flames. Int J Hydrogen Energy 2012;38:8141–58. https://doi.org/10.1016/j.ijhydene.2012.08.106.

[26] Malakhov AA, Avdeenkov A V., du Toit MH, Bessarabov DG. CFD simulation and experimental study of a hydrogen leak in a semi-closed space with the purpose of risk mitigation. Int J Hydrogen Energy 2020;45:9231–40. https://doi.org/10.1016/j.ijhydene.2020.01.035.

[27] Uriz I, Arzamendi G, Dieguez PM, Gandia LM. Computational Fluid Dynamics as a Tool for Designing Hydrogen. In: Gandia LM, Arzamendi G, Dieguez PM, editors. Renew. Hydrog. Technol. Prod. Purification, Storage, Appl. Saf., UK: Elsevier; 2013. https://doi.org/https://doi.org/10.1016/B978-0-444-56352-1.00017-9.

[28] Choi J, Hur N, Kang S, Lee ED, Lee KB. A CFD simulation of hydrogen dispersion for the hydrogen leakage from a fuel cell vehicle in an underground parking garage. Int J Hydrogen Energy 2013;38:8084–91. https://doi.org/10.1016/j.ijhydene.2013.02.018.

[29] Giannissi SG, Shentsov V, Melideo D, Cariteau B, Baraldi D, Venetsanos AG, et al. CFD benchmark on hydrogen release and dispersion in confined, naturally ventilated space with one vent. Int J Hydrogen Energy 2015;40:2415–29. https://doi.org/10.1016/j.ijhydene.2014.12.013.

[30] Giannissi SG, Venetsanos AG. Study of key parameters in modeling liquid hydrogen release and dispersion in open environment. Int J Hydrogen Energy 2018;43:455–67. https://doi.org/10.1016/j.ijhydene.2017.10.128.

[31] Tolias IC, Giannissi SG, Venetsanos AG, Keenan J, Shentsov V, Makarov D, et al. Best practice guidelines in numerical simulations and CFD benchmarking for hydrogen safety applications. Int J Hydrogen Energy 2019;44:9050–62. https://doi.org/10.1016/j.ijhydene.2018.06.005.

[32] Larsson M, Santos G, Turoń K, Alanne K, Cao S, Rogié B, et al. Hydrogen production for energy: An overview. Int J Hydrogen Energy 2019;45:71–4. https://doi.org/10.1016/j.ijhydene.2016.06.167.

[33] Venetsanos AG, Papanikolaou E, Delichatsios M, Garcia J, Hansen OR, Heitsch M, et al. An inter-comparison exercise on the capabilities of CFD models to predict the short and long term distribution and mixing of hydrogen in a garage. Int J Hydrogen Energy 2009;34:5912–23. https://doi.org/10.1016/j.ijhydene.2009.01.055.

[34] Salva JA, Tapia E, Iranzo A, Pino FJ, Cabrera J, Rosa F. Safety study of a hydrogen leak in a fuel cell vehicle using computational fluid dynamics. Int J Hydrogen Energy 2012;37:5299–306. https://doi.org/10.1016/j.ijhydene.2011.12.046.

[35] Benintendi R, Turns SR, Deimling L, Weiser V, Blanc A, Eisenreich N, et al. Fundamentals of Hydrogen Safety Engineering I Download free books at Vladimir Molkov Fundamentals of Hydrogen Safety Engineering I. Int J Hydrogen Energy 2012;36:12254–69. https://doi.org/10.1016/j.ijhydene.2019.03.041.

[36] Houf WG, Evans GH, Schefer RW. Analysis of jet flames and unignited jets from unintended releases of hydrogen. Int J Hydrogen Energy 2009;34:5961–9. https://doi.org/10.1016/j.ijhydene.2009.01.054.

[37] Wang CJ, Wen JX, Chen ZB, Dembele S. Predicting radiative characteristics of hydrogen and hydrogen/methane jet fires using FireFOAM. Int J Hydrogen Energy 2014;39:20560–9. https://doi.org/10.1016/j.ijhydene.2014.04.062.

[38] Bie HY, Hao ZR. Simulation analysis on the risk of hydrogen releases and combustion in subsea tunnels. Int J Hydrogen Energy 2017;42:7617–24. https://doi.org/10.1016/j.ijhydene.2016.05.263.

[39] He J, Kokgil E, Wang L (Leon), Ng HD. Assessment of similarity relations using helium for prediction of hydrogen dispersion and safety in an enclosure. Int J Hydrogen Energy 2016;41:15388–98. https://doi.org/10.1016/j.ijhydene.2016.07.033.

[40] Pitts WM, Yang JC, Blais M, Joyce A. Dispersion and burning behavior of hydrogen released in a full-scale residential garage in the presence and absence of conventional automobiles. Int J Hydrogen Energy 2012;37:17457–69. https://doi.org/10.1016/j.ijhydene.2012.03.074.

[41] Zhang Q, Liang D, Wen J. Experimental study of flashing LNG jet fires following horizontal releases. J Loss Prev Process Ind 2019;57:245–53. https://doi.org/10.1016/j.jlp.2018.12.007.

[42] Pio G, Carboni M, Salzano E. Realistic aviation fuel chemistry in computational fluid dynamics. Fuel 2019;254:115676. https://doi.org/10.1016/j.fuel.2019.115676.

[43] Hess K, Leuckel W, Stoeckel A. Ausbildung von Explosiblen Gaswolken bei Uberdachtspannung und MaBnahmen zu deren Vermeidung. Chem Ing Tech 1973;45:5323–9.

[44] Turns SR. An introduction to combustion. n.d.

[45] van den Bosch C, Weterings R. Yellow Book - Methods for the calculation of physical effects due to releases of hazardous materials (liquids and gases). CPR 14E, 3rd Edn, TNO 1997.

[46] ANSYS Fluent Software: CFD Simulation n.d.:http://ansys. com/products/fluids/ansys-fluent.

[47] Chamberlain GA. Developments in design methods for predicting thermal radiation from flares. Chem Eng Res Des 1987;65:299–309.

[48] Cook J, Bahrami Z, Whitehouse RJ. A comprehensive program for calculation of flame radiation levels. J Loss Prev Process Ind 1990;3:150–5. https://doi.org/10.1016/0950-4230(90)85039-C

[49] Launder B. E., B. SD. MAN - ANSYS Fluent User' s Guide Releasde 15.0. Knowl Creat Diffus Util 2013;15317:724–46.

[50] Salzano E, Carboni M, Pio G. The effects of low-temperature phenomena on rapid phase transition of liquid hydrogen. Int J Hydrogen Energy 2020;45:32676–85. https://doi.org/10.1016/j.ijhydene.2020.08.140.

[51] Burcat A, Branko R. Third millennium ideal gas and condensed phase thermochemical database for combustion with updates from active thermochemical tables. Tech Rep 2005;ANL-05/20:ANL-05/20 TAE 960. https://doi.org/10.2172/925269.

[52]   Barlow RS, Carter CD. Relationship among Nitric Oxide, Temperature, and Mixture Fraction in Hydrogen Jet Flames. Combust Flame n.d.;104:288–99.

[53]   LaChance J. Risk-informed separation distances for hydrogen refueling stations. Int J Hydrogen Energy 2009;34:5838–45. https://doi.org/10.1016/j.ijhydene.2009.02.070.

[54]   Delichatsios MA. Transition from momentum to buoyancy-controlled turbulent jet diffusion flames and flame height relationships. Combust Flame 1993;92:349–64. https://doi.org/10.1016/0010-2180(93)90148-V.

[55]   Mocellin P, Maschio G. Numerical modeling of experimental trials involving pressurized release of gaseous co2. Chem Eng Trans 2016;53:349-354. https://doi.org/10.3303/CET1653059.